arXiv:1511.01227v1 [math.DS] 4 Nov 2015

Periodic Orbits for a Discontinuous Vector Field Arising from a Conceptual Model of Glacial Cycles

James Walsh
Department of Mathematics, Oberlin College

Esther Widiasih
Department of Mathematics, University of Hawaii–West Oahu

Jonathan Hahn
School of Mathematics, University of Minnesota

Richard McGehee
School of Mathematics, University of Minnesota

July 20, 2015

Abstract. Conceptual climate models provide an approach to understanding climate processes through a mathematical analysis of an approximation to reality. Recently, these models have also provided interesting examples of nonsmooth dynamical systems. Here we discuss a conceptual model of glacial cycles consisting of a system of three ordinary differential equations defining a discontinuous vector field. We show that this system has a large periodic orbit crossing the discontinuity boundary. This orbit can be interpreted as an intrinsic cycling of the Earth's climate giving rise to alternating glaciations and deglaciations.

1 Introduction

In recent years an extensive theory of discontinuous differential equations has been built, based largely on the work of Filippov [7]. Although the general theory is far from complete [9], it is sufficiently developed to allow it to be applied to systems such as the model of glacial cycles described here.

Conceptual models of the Earth's ice sheets began with the work of Budyko [5] and Sellers [28]. Using a simple equation incorporating latitudinal variation of the incoming

solar radiation and the ice-albedo feedback effect, Budyko was able to show the existence of a stable small ice cap. Widiasih [33] introduced an equation for the motion of the edge of the ice sheet (called the ice line), enabling the use of dynamical systems theory to examine the ice line dynamics. Subsequently, she and McGehee [18] introduced an approximation to the Budyko-Widiasih model, reducing the model to a system of two ordinary differential equations.

Many aspects of the Earth's glacial cycles remain a mystery. For roughly the last million years, the Earth's climate has experienced extensive cold periods with large ice sheets covering much of North America and Eurasia. These glacial periods have been followed by relatively rapid transitions to warmer temperatures as the ice sheets retreat. These so-called interglacial periods, which are shorter in duration, are typically followed by a slow descent into the subsequent glacial period, leading to the asymmetric sawtooth pattern evident in the paleoclimate data [26]. These glacial/interglacial cycles have occurred with a periodicity of roughly 100,000 years.

The explanation for the 100,000 year cycles usually appeals in some way to the work of Milankovitch [19], who examined the impact of variations in the Earth's orbital parameters on the incoming solar radiation (called Milankovitch cycles). It turns out that the eccentricity of the Earth's orbit changes with a period of about 100,000 years, corresponding with the glacial cycles of the last million years. However, the paleoclimate record shows that, for the period between five million and one million years ago, the glacial cycles occurred with a period of about 41,000 years, corresponding instead to changes in the Earth's obliquity (axial tilt). Since the Milankovitch cycles have not changed significantly over the last five million years, it is clear that the Earth's climate cycles cannot be explained as a simple response to the Milankovitch forcing.

Many models have been proposed to explain the response of the Earth's climate to the Milankovitch cycles. One of the earliest was in a paper of Maasch and Saltzman [16], where they proposed that, for the last million years, the Earth's climate system has had an intrinsic oscillation of 100,000 years, independent of the Milankovitch cycles. Dynamically speaking, the autonomous system has a stable periodic orbit with a period of about 100,000 years. When the Milankovitch cycles are introduced, the system becomes nonautonomous and falls into synchronization with the eccentricity cycles. The change that occurred one million years ago can be explained as slow changes in the parameters of the Earth's climate system creating a Hopf bifurcation in the autonomous system, changing the response to the forcing.

Many other conceptual models have been introduced to study nonlinear climate feedbacks as they relate to the glacial cycles. These models often include a threshold that, once exceeded, triggers a switch from, say, a glacial to an interglacial period. In previous studies the threshold variable has been ice volume [12], [13]; a combination of

Milankovitch forcing and ice volume [22], [24]; a function of ice volume, Milankovitch forcing and area of the Antarctic ice sheet [23]; and a switch connected to the rapid formation of sea ice [29]. In related work, a relaxation model is subjected to astronomical forcing to produce oscillations in global ice volume in [2]. In many of these works, model parameters are adjusted in attempts to generate output that qualitatively mirrors the paleoclimate data.

Starting with the McGehee-Widiasih version of Budyko's equation [18] and inspired by the work of Källén et al [14], we consider Widiasih's ice line variable to be the albedo line, where the snow cover remains throughout the year, and introduce a new variable, corresponding to the extent of the ice sheet. The thinking here is that, during the glacial advance, the snow is accumulating (forming the glacier) at a lower latitude than the ice sheet edge, and hence that the albedo line is at a lower latitude than the ice sheet edge. On the other hand, the work of Wright and Stefanova [34] indicates that, during the glacial retreat, forests growing on top of the retreating ice sheets create an albedo line at a higher latitude than the edge of the ice sheet. These phenomena give rise to what we think of as two distinct climate regimes, one occurring during the glacial advance and the other occurring during the glacial retreat. The boundary between these two regimes corresponds to a discontinuity in the vector field, allowing us to view the model as a Filippov system.

Our model is a system of three ordinary differential equations with a discontinuity boundary consisting of a plane in the three-dimensional state space. Using techniques reminiscent of singular perturbation theory, we show the existence of a large periodic orbit crossing the discontinuity boundary.

In terms of the theory of glacial cycles, this work represents only the beginning, analogous to the establishment of a periodic orbit in the Maasch and Satzman model. Missing is an analysis of the response to the Milankovitch forcing. The forcing will be easy to introduce into the model, since it is based on the Budyko model, where the Milankovitch cycles can be easily incorporated [17].

In terms of the mathematical theory, there may be some work to be done in studying the response of a Filippov system to time variation of the parameters. In addition, our analysis points to the need to develop a theory of singular perturbations for Filippov systems.

The paper is organized as follows. In the next section we introduce Budyko's model and its coupling with a dynamic ice line. In Section 3 we review the quadratic approximation introduced in [18], which we then augment by including a snow line independent of the edge of the ice sheet, as presented in Section 4. This in turn leads to a discontinuous three-dimensional vector field, the dynamics of which we analyze in Section 5. We point to several problems of mathematical interest generated by the study of the model

and we summarize this work in the concluding section.

2 A coupled temperature-ice line model

Budyko's energy balance model concerns the average annual temperature in latitudinal zones in a world assumed to be symmetric about the equator. While Budyko focused solely on equilibrium temperature distributions, we consider the time-dependent equation [11]

$$R\frac{\partial T(y,t)}{\partial t} = Qs(y)(1-\alpha(y)) - (A+BT) - C(T-\overline{T}). \tag{1}$$

In equation (1), y is the sine of the latitude, chosen for convenience (the area of an infinitesimal latitudinal strip at y is proportional to dy). Note that due to symmetry considerations, $y \in [0,1]$, with $y=0$ the equator and $y=1$ the North Pole.

The function $T = T(y,t)$ (°C) is the annual mean surface temperature on the circle of latitude at y, and R is the heat capacity of the Earth's surface (with units J/(m^2 °C)). The left-hand side of (1) represents the change in energy stored in the Earth's surface at y; units on each side of (1) are Watts per meter squared (W/m^2).

Q denotes the mean annual incoming solar radiation (or *insolation*), a parameter depending on the eccentricity of Earth's orbit [17]. The function $s(y)$, which depends upon the obliquity of Earth's orbit [17], accounts for the distribution of insolation across latitude, and satisfies

$$\int_0^1 s(y)dy = 1.$$

The function $\alpha(y)$ represents the planetary *albedo*, a measure of the extent to which insolation is reflected back into space. Thus the $Qs(y)(1-\alpha(y))$-term represents the energy from the sun absorbed at the surface at "latitude" y.

The $(A+BT)$-term models the *outgoing longwave radiation* (OLR) emitted by the Earth, while the transport of heat energy across latitudes is modeled by the $C(T-\overline{T})$-term, in which

$$\overline{T} = \int_0^1 T(y,t)dy$$

is the global annual mean surface temperature. The constants A, B and C are positive and empirical (for a more detailed introduction to Budyko's EBM see [18], [30]).

In [18] the equilibrium temperature profiles of (1) are shown to be given by

$$T^*(y) = \frac{1}{B+C}\left(Qs(y)(1-\alpha(y)) - A + \frac{C}{B}(Q(1-\overline{\alpha}) - A)\right), \tag{2}$$

where

$$\overline{\alpha} = \int_0^1 \alpha(y)s(y)dy. \tag{3}$$

Letting $p_0(y) = 1$ and $p_2(y) = \frac{1}{2}(3y^2-1)$ denote the first two even Legendre polynomials, we make use of the expression

$$s(y) = s_0 p_0(y) + s_2 p_2(y),\ s_0 = 1,\ s_2 = -0.482, \tag{4}$$

which is uniformly within 2% of the actual values of $s(y)$ [20], in all that follows.

In Budyko's model one assumes the planet has an ice cap, with ice at all latitudes above a certain latitude $y = \eta$, and no ice south of $y = \eta$. The edge of the ice sheet η is called the *ice line*. The albedo function is then given by

$$\alpha_\eta(y) = \begin{cases} \alpha_1, & \text{if } \ y < \eta \\ \alpha_2, & \text{if } \ y > \eta, \end{cases} \qquad \alpha_1 < \alpha_2, \tag{5}$$

where α_1 and α_2 represent the albedos of surface with no ice cover and that having an ice cover, respectively. With this choice of albedo function, and using expression (4), equilibrium temperature profiles (2) are even, piecewise quadratic functions having a discontinuity at η. We also note η serves to parametrize (3), and hence equilibrium functions (2), as well. In particular, there are infinitely many equilibrium temperature functions, one for each value of η. We write $T^*_\eta(y)$ when we wish to emphasize this parametrization.

Defining $T^*_\eta(\eta) = \frac{1}{2}(\lim_{y\to\eta^-} T^*(y) + \lim_{y\to\eta^+} T^*(y))$, one finds the temperature at equilibrium at the ice line is given by

$$T^*_\eta(\eta) = \frac{1}{B+C}\left(Qs(\eta)(1-\alpha_0) - A + \frac{C}{B}(Q(1-\overline{\alpha}(\eta) - A)\right), \tag{6}$$

with $\alpha_0 = \frac{1}{2}(\alpha_1 + \alpha_2)$. Budyko was interested in the existence of η-values for which $T^*_\eta(\eta) = T_c$, where T_c is a *critical temperature* above which ice melts and below which ice forms. Specifically, he investigated the relationship between the number of such η-values and the parameter Q.

As mentioned in the introductory section, Budyko was motivated by the study of the positive ice-albedo feedback: If temperatures were to decrease, an existing ice sheet would grow, increasing the albedo and further lowering temperatures, leading to an ever larger ice sheet. A warming climate would lead to a smaller ice sheet and reduced albedo, thereby raising temperatures and further reducing the size of the ice sheet.

Budyko found that for a range of Q-values there exist $\eta_1 < \eta_2$ with $T^*_{\eta_i}(\eta_i) = T_c = -10°\text{C}$, $i = 1, 2$, with η_1 in lower latitudes and η_2 nearer the North Pole. If Q decreased

sufficiently, however, there were no such η-values, with the implication being that the ice line would be positioned at the equator for these Q-values (a so-called *Snowball Earth* event). This was viewed as a consequence of ice-albedo feedback. Notably, previous analyses of Budyko's model lacked any treatment of the stability of the "preferred" equilibrium temperature distributions having $T_\eta^*(\eta) = T_c$ (or, indeed, of $T_\eta^*(y)$ for any η) from a dynamical systems perspective, that is, in the infinite-dimensional setting intrinsic to (1).

Additionally, Budyko's model lacks any mechanism by which the ice line η is allowed to respond to changes in temperature. This limitation was remedied by E. Widiasih in [33] through the addition of an ODE for the evolution of η, leading to the integro differential system

$$R\frac{\partial T}{\partial t} = Qs(y)(1-\alpha(y,\eta)) - (A+BT) - C(T-\overline{T}) \tag{7a}$$

$$\frac{d\eta}{dt} = \rho(T(\eta,t) - T_c). \tag{7b}$$

Here, $\rho > 0$ is a parameter governing the relaxation time of the ice sheet. The temperature distribution $T(y,t)$ evolves according to Budyko's equation (7a), while the dynamics of η are determined by the temperature at the ice line, relative to the critical temperature. The ice sheet retreats toward the pole if $T(\eta,t) > T_c$, and moves equatorward if $T(\eta,t) < T_c$.

Working in the infinite-dimensional setting and with parameters as in Budyko's work, Widiasih proved the existence of equilibrium temperature–ice line pairs $(T_{\eta_i}(y), \eta_i), i = 1,2$, for ρ sufficiently small. The ice line $y = \eta_2$ corresponds to a stable, small ice cap, while ice line $y = \eta_1$ corresponds to a large, unstable ice sheet (in particular, there are no oscillations of the ice sheet in the model). This work provided Budyko's pioneering and influential model with a modern dynamical systems perspective.

3 The approximation of McGehee and Widiasih

Recall equilibrium solutions of Budyko's equation (1) are even and piecewise quadratic, with a discontinuity at η, when using albedo function (5) and expression (4). This motivated the introduction of a quadratic approximation to system (7) in [18]. We outline this approach here, referring the reader to [18] for all computational details.

Let X denote the space of even, piecewise quadratic functions having a discontinuity at η. The four-dimensional linear space X can be parametrized by the new variables

w_0, z_0, w_2 and z_2 by letting

$$T(y) = \begin{cases} w_0 + \frac{1}{2}z_0 + (w_2 + \frac{1}{2}z_2)p_2(y), & y < \eta \\ w_0 - \frac{1}{2}z_0 + (w_2 - \frac{1}{2}z_2)p_2(y), & y > \eta \\ w_0 + w_2 p_2(\eta), & y = \eta. \end{cases} \tag{8}$$

The choice of $T(\eta)$ in (8) coincides with $T(\eta) = \frac{1}{2}(\lim_{y\to\eta^-} T(y) + \lim_{y\to\eta^+} T(y))$, to maintain consistency with (6). One can show that, in these variables,

$$\overline{T} = \int_0^1 T(y)dy = w_0 + z_0(\eta - \tfrac{1}{2}) + z_2 P_2(\eta), \text{ where } P_2(\eta) = \int_0^\eta p_2(y)dy. \tag{9}$$

Plugging (8) and (4) into (1) and equating the coefficients of $p_0(y)$ (that is, the constant terms) and $p_2(y)$, respectively, yields the four equations

$$R(\dot{w}_0 + \tfrac{1}{2}\dot{z}_0) = Q(1-\alpha_1) - A - (B+C)(w_0 + \tfrac{1}{2}z_0) + C\overline{T} \tag{10a}$$
$$R(\dot{w}_0 - \tfrac{1}{2}\dot{z}_0) = Q(1-\alpha_2) - A - (B+C)(w_0 - \tfrac{1}{2}z_0) + C\overline{T} \tag{10b}$$
$$R(\dot{w}_2 + \tfrac{1}{2}\dot{z}_2) = Qs_2(1-\alpha_1) - (B+C)(w_2 + \tfrac{1}{2}z_2) \tag{10c}$$
$$R(\dot{w}_2 - \tfrac{1}{2}\dot{z}_2) = Qs_2(1-\alpha_2) - (B+C)(w_2 - \tfrac{1}{2}z_2) \tag{10d}$$

(two equations each for $y < \eta$ and $y > \eta$). Adding and subtracting equations (10a)-(10b) and (10c)-(10d) and substituting in expression (9) for $\overline{T}$, one arrives at

$$\begin{aligned} R\dot{w}_0 &= Q(1-\alpha_0) - A - Bw_0 + C((\eta - \tfrac{1}{2})z_0 + z_2 P_2(\eta)) \\ R\dot{z}_0 &= Q(\alpha_2 - \alpha_1) - (B+C)z_0 \\ R\dot{w}_2 &= Qs_2(1-\alpha_0) - (B+C)w_2 \\ R\dot{z}_2 &= Qs_2(\alpha_2 - \alpha_1) - (B+C)z_2. \end{aligned} \tag{11}$$

Let $L = Q/(B+C)$. Note system (11) admits a globally attracting invariant line $\mathcal{L}$ on which

$$z_0 = L(\alpha_2 - \alpha_1), \; w_2 = Ls_2(1-\alpha_0), \text{ and } z_2 = Ls_2(\alpha_2 - \alpha_1)$$

are each at equilibrium. One can show that on $\mathcal{L}$ system (11) reduces to the single equation

$$R\dot{w} = -B(w - F(\eta)), \tag{12}$$

where we have let $w = w_0$ for ease of notation, and where

$$F(\eta) = \frac{1}{B}\left(Q(1-\alpha_0) - A + CL(\alpha_2 - \alpha_1)(\eta - \tfrac{1}{2} + s_2 P_2(\eta))\right). \tag{13}$$

We note $F(\eta)$ is a cubic polynomial. Thus, equation (12) provides the approximation to equation (7a).

For equation (7b), one computes the expression for $T(\eta)$ on the invariant line $\mathcal{L}$. As detailed in [18], equation (7b) can be written in the form

$$\dot{\eta} = \rho(w - G(\eta)),$$

where

$$G(\eta) = -Ls_2(1 - \alpha_0)p_2(\eta) + T_c, \tag{14}$$

when restricting to $\mathcal{L}$. Hence the infinite-dimensional system (7) is approximated by the system of ODEs

$$\begin{aligned} \dot{w} &= -\tau(w - F(\eta)) \\ \dot{\eta} &= \rho(w - G(\eta)), \end{aligned} \tag{15}$$

with $F(\eta)$ given by (13), $G(\eta)$ the quadratic polynomial (14), and $\tau = B/R$. One can show that for fixed η the variable w is a translate of the global average temperature [18].

Phase planes for system (15) are shown in Figure 1. Note the existence of equilibrium solutions is independent of ρ and τ. Moreover, in [18] it is shown that there exist a stable equilibrium point with ice line near the pole, and a saddle equilibrium point with a large ice cap, for all $\rho > 0$ (as in Figure 1(a)), for standard parameter values (also see §5.1). This simple two-dimensional model captures the essence of the dynamics of the infinite-dimensional Budyko-Widiasih model (7).

As mentioned above, system (15) does not allow for glacial cycles, given that η either approaches an equilibrium position or the equator over time. Motivated by the role played by the relative sizes of the accumulation and ablation zones in glacial advance and retreat, we introduce a new snow line variable, independent of the edge of the ice sheet, thereby supplementing equations (15). We present this model in the following section.

4 Addition of a snow line

The accumulation and ablation of ice play a fundamental role in the theory of glacial cycles, serving to control the terminus advance and retreat, the ice volume, and the geometry of the surface of the ice sheet [3]. Significant motivation for our model stems from the study [1], in which numerical simulations of the glacial cycles over the past 400 kyr were carried out using an ice sheet model coupled to a general circulation model. These simulations typically produced two stable equilibrium ice line positions for a given

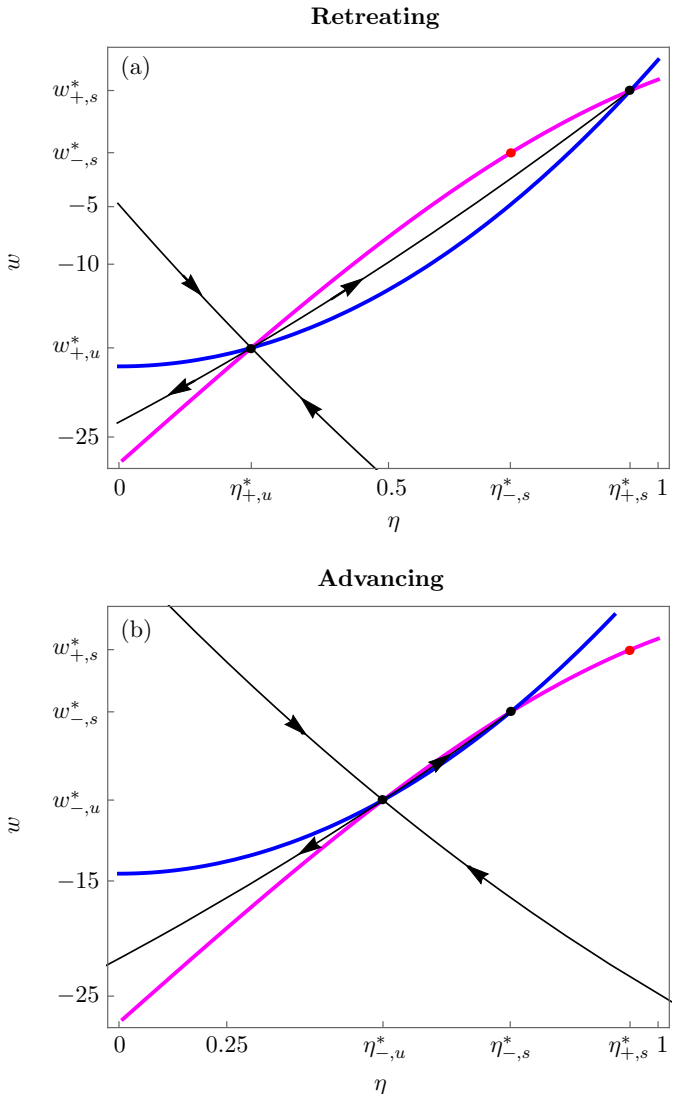

Figure 1: (a) Phase plane for the subsystem (17a)-(17b), for which $T_c^+ = -10°\text{C}$. (b) Phase plane for the subsystem (16a)-(16b), for which $T_c^- = -5.5°\text{C}$. In each plot the magenta curve is the w-nullcline, and the blue curve is the η-nullcline. The η-nullcline in (b) is the η-nullcline in (a) translated vertically by $T_c^- - T_c^+$. The w-nullclines in (a) and (b) are identical.

set of parameters, one small and the other much larger. In addition, the larger the ice sheet at equilibrium, the larger was the ablation zone, leading to increased ice sheet instability with regard to Milankovitch forcing.

Most importantly, however, Abe-Ouchi et al found the fast retreat of the ice sheet was due to significantly enhanced ablation (due in turn to delayed isostatic rebound [1]). That is, the ablation rate for a large, advancing ice sheet was necessarily much smaller than the ablation rate for a retreating ice sheet, in order to faithfully reproduce the last four glacial cycles. We incorporate this simple idea into our conceptual model below. For further insight into the important role played by ablation rates (and the ratio of ablation rates to accumulation rates) in modeling glacial cycles see, for example, [8], [14], [21], [27], [29], [31].

Motivation for our model was also drawn from a model of the thermohaline circulation presented in [32]. This simple "flip-flop" conceptual model exhibits oscillations in the temperature and salinity of a well-mixed ocean layer. The model vector field has a line of discontinuity that produces a switch to the alternate regime when intersected by a trajectory. Similarities between our model and that presented in [32] will become evident below.

Consider once again system (15). Recall that for fixed η-values, w is a translate of the global average temperature. We introduce independent snow and ice lines so as to incorporate accumulation and ablation zones. The model continues to depend upon latitude as discussed in Sections 2 and 3.

We begin by recasting the role played by η, interpreting η henceforth as the snow line. We let ξ denote the ice line, that is, the edge of the ice sheet (see Figure 2). The ablation zone has extent $\eta - \xi$ (when $\eta > \xi$), while the accumulation zone has size $1 - \eta$.

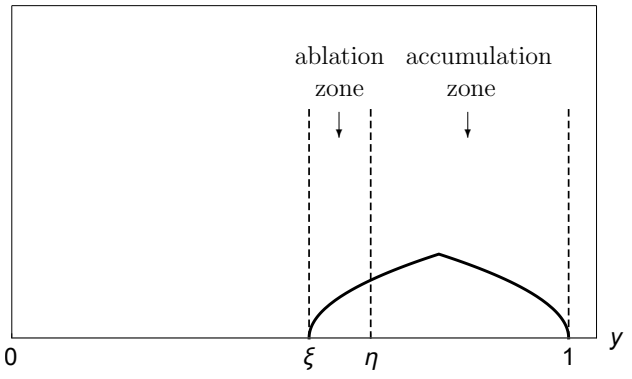

Figure 2: The model set-up. η is the snow line and ξ is the ice line. The shape of the glacier is for illustrative purposes only.

We continue to use albedo function (5). We note the albedo of the portion of the ice sheet in the ablation zone is much smaller than that of the ice sheet lying poleward of η. For example, as the old ice emerges and melts in the ablation zone, a surface layer of dust that was originally laid down with snowfall high on the ice sheet is created [4]. Additionally, locally increased winds further cover the surface in the ablation zone with dust and debris [25]. Albedo value α_1 in (5) might then be interpreted as an average of the albedos of the planet's surface south of ξ and the darkened (relative to snow) ice surface in the ablation zone.

The use of independent ice and snow lines was also partially due to the desire to include ice volume in this latitude-dependent model. (A strong argument for the inclusion of ice volume in any EBM is given in [21].) While our model does not explicitly include volume, the latter can be recovered from ξ were we to assume a specific ice sheet shape as, for example, in [31]. Finally, the model allows for different time scales for the snow line and the (more slowly moving) ice line.

4.1 Model equations

The temperature-ice line-snow line model is a nonsmooth system with state space

$$\mathcal{B} = \{(w, \eta, \xi) : w \in \mathbb{R}, \eta \in [0, 1], \xi \in [0, 1]\},$$

defined as follows. Pick parameters $b_0 < b < b_1$ representing ablation rates, and a parameter a denoting the accumulation rate. When $b(\eta - \xi) - a(1 - \eta) < 0$, so that accumulation exceeds ablation and the ice sheet advances, set

$$\dot{w} = -\tau(w - F(\eta)) = f_1^-(w, \eta, \xi) \tag{16a}$$
$$\dot{\eta} = \rho(w - G_-(\eta)) = f_2^-(w, \eta, \xi) \tag{16b}$$
$$\dot{\xi} = \epsilon(b_0(\eta - \xi) - a(1 - \eta)) = f_3^-(w, \eta, \xi). \tag{16c}$$

The function $F(\eta)$ in (16a) is given by (13), $G_-(\eta)$ in (16b) is given by (14) but with $T_c = T_c^- = -5.5°\text{C}$, and $\epsilon > 0$ is a time constant for the movement of the ice line.

When ablation exceeds accumulation ($b(\eta - \xi) - a(1 - \eta) > 0$) and the ice sheet retreats, we set

$$\dot{w} = -\tau(w - F(\eta)) = f_1^+(w, \eta, \xi) \tag{17a}$$
$$\dot{\eta} = \rho(w - G_+(\eta)) = f_2^+(w, \eta, \xi) \tag{17b}$$
$$\dot{\xi} = \epsilon(b_1(\eta - \xi) - a(1 - \eta)) = f_3^+(w, \eta, \xi). \tag{17c}$$

The function $F(\eta)$ in (17a) is again given by (13), while $G_+(\eta)$ in (17b) is given by (14)

with $T_c = T_c^+ = -10°\text{C}$.

The relative sizes of ablation rates b_0 and b_1 were motivated by [1] as described above. The choice of different T_c-values is motivated by [29], in which a linear interpolation between $T_c = -13°\text{C}$ and $T_c = -3°\text{C}$ is introduced to model changes in deep ocean temperature. The intuitive idea is that a large advancing ice sheet implies a colder world generally, so that less energy is require to form ice (and vice versa for a retreating ice sheet).

We thus arrive at a three-dimensional system having a plane of discontinuity

$$\Sigma = \{\, (w,\eta,\xi) : b(\eta-\xi) - a(1-\eta) = 0 \,\} = \{\, (w,\eta,\xi) : \xi = (1+\tfrac{a}{b})\eta - \tfrac{a}{b} \equiv \gamma(\eta) \,\}. \quad (18)$$

As we will see, a trajectory in (w,η,ξ)-space passing through Σ switches from advancing mode to glacial retreat, or vice versa, similar in spirit to the flip-flop model in [32].

Let

$$S_+ = \{\, (w,\eta,\xi) \in \mathcal{B} : \xi < \gamma(\eta) \,\} \quad \text{and} \quad S_- = \{\, (w,\eta,\xi) \in \mathcal{B} : \xi > \gamma(\eta) \,\},$$

with $\gamma(\eta)$ as in (18). Called a *discontinuity boundary* (or *switching boundary*), Σ is a hyperplane separating $\mathcal{B}$ into subspaces S_+ and S_-. Consider the vector fields

$$\mathbf{V}_\pm : S_\pm \to \mathbb{R}^3,\ \mathbf{V}_\pm(w,\eta,\xi) = (f_1^\pm(w,\eta,\xi), f_2^\pm(w,\eta,\xi), f_3^\pm(w,\eta,\xi)),$$

noting $\mathbf{V}_\pm$ each extend smoothly to Σ. For $\mathbf{x} = (w,\eta,\xi) \in \mathcal{B}$, consider the differential inclusion

$$\dot{\mathbf{x}} \in \mathbf{V}(\mathbf{x}) = \begin{cases} \mathbf{V}_-(\mathbf{x}), & \mathbf{x} \in S_- \\ \{(1-q)\mathbf{V}_-(\mathbf{x}) + q\mathbf{V}_+(\mathbf{x}) : q \in [0,1]\}, & \mathbf{x} \in \Sigma \\ \mathbf{V}_+(\mathbf{x}), & \mathbf{x} \in S_+. \end{cases} \quad (19)$$

Solutions, while in S_-, have flow $\phi_-(\mathbf{x},t)$ given by $\dot{\mathbf{x}} = \mathbf{V}_-(\mathbf{x})$, and solutions have flow $\phi_+(\mathbf{x},t)$ given by $\dot{\mathbf{x}} = \mathbf{V}_+(\mathbf{x})$ while in S_+. For $\mathbf{x} \in \Sigma$, $\dot{\mathbf{x}}$ must lie in the closed convex hull of the two vectors $\mathbf{V}_-(\mathbf{x})$ and $\mathbf{V}_+(\mathbf{x})$.

A solution to (19) *in the sense of Filippov* is an absolutely continuous function $\mathbf{x}(t)$ satisfying $\dot{\mathbf{x}} \in \mathbf{V}(\mathbf{x})$ for almost all t. (Note $\dot{\mathbf{x}}(t)$ is not defined at times for which $\mathbf{x}(t)$ arrives at or leaves Σ.) Given that $\mathbf{V}_\pm$ are continuous on $S_\pm \cup \Sigma$, the set-valued map $\mathbf{V}(\mathbf{x})$ is upper semi-continuous, and closed, convex and bounded for all $\mathbf{x} \in \mathcal{B}$ and $t \in \mathbb{R}$. This implies that for each $\mathbf{x}_0 \in \text{Int}(\mathcal{B})$ there is a solution $\mathbf{x}(t)$ to differential inclusion (19) in the sense of Filippov, defined on an interval $[0, t_f]$, with $\mathbf{x}(0) = \mathbf{x}_0$ [15].

We now turn to an analysis of the model.

5 Model analysis

We first note model equations (16) and (17) partially decouple: As long as a trajectory remains in S_- or S_+, changes in ξ play no role in the evolution of w and η. This simple observation will prove useful in the following analysis.

We set several parameter values before continuing.

Parameter	Value	Units	Parameter	Value	Units
Q	343	Wm^{-2}	T_c^-	-5.5	°C
A	202	Wm^{-2}	b_0	1.5	dimensionless
B	1.9	$\mathrm{Wm}^{-2}(^\circ\mathrm{C})^{-1}$	b	1.75	dimensionless
C	3.04	$\mathrm{Wm}^{-2}(^\circ\mathrm{C})^{-1}$	b_1	5	dimensionless
α_1	0.32	dimensionless	a	1.05	dimensionless
α_2	0.62	dimensionless	τ	1	$\mathrm{seconds}^{-1}$
T_c^+	-10	°C	ρ	0.1	$\mathrm{seconds}^{-1}(^\circ\mathrm{C})^{-1}$

Table 1 Parameter values (left column from [18]). The parameter ϵ has units $(\mathrm{seconds})^{-1}$.

5.1 Equilibria

Note time constants τ, ρ and ϵ play no role in the determination of equilibrium solutions of systems (16) and (17). As we'll see below, they also play no role in determining the stability type of any equilibria.

An equilibrium point $\mathbf{Q}_+^* = (w_+^*, \eta_+^*, \xi_+^*)$ for (17) satisfies $w_+^* = F(\eta_+^*) = G_+(\eta_+^*)$ (that is, $F(\eta_+^*) - G_+(\eta_+^*) = 0$), and $\xi_+^* = (1 + \frac{a}{b_1})\eta_+^* - \frac{a}{b_1}$. In [18] it was shown that, with parameters as in Table 1, the (decoupled) subsystem (17a)-(17b) has a "small ice cap" sink $(w_{+,s}^*, \eta_{+,s}^*) \approx (5.08, 0.95)$ and a "large ice cap" saddle $(w_{+,u}^*, \eta_{+,u}^*) \approx (-17.26, 0.25)$ (see Figure 1(a)), and no other equilibria having $\eta \in [0, 1]$. Hence system (17) has two equilibria

$$\mathbf{Q}_{+,s}^* = (w_{+,s}^*, \eta_{+,s}^*, (1 + \tfrac{a}{b_1})\eta_{+,s}^* - \tfrac{a}{b_1}) \quad \text{and} \quad \mathbf{Q}_{+,u}^* = (w_{+,u}^*, \eta_{+,u}^*, (1 + \tfrac{a}{b_1})\eta_{+,u}^* - \tfrac{a}{b_1}).$$

The Jacobian matrix for (17) is

$$J_+(w, \eta, \xi) = \begin{bmatrix} -\tau & \tau F'(\eta) & 0 \\ \rho & -\rho G'_+(\eta) & 0 \\ 0 & \epsilon(b_1 + a) & -\epsilon b_1 \end{bmatrix}. \tag{20}$$

Thus at any equilibrium point $\mathbf{Q}^*$, $-\epsilon b_1$ is an eigenvalue of $J_+(\mathbf{Q}^*)$ with eigenvector $[0\ 0\ 1]^T$. Combining this with the analysis in [18], we see that $J_+(\mathbf{Q}_{+,s}^*)$ has three negative

eigenvalues, while $J_+(\mathbf{Q}^*_{+,u})$ has two negative eigenvalues and one positive eigenvalue. We have that $\mathbf{Q}^*_{+,s}$ is a sink, and $\mathbf{Q}^*_{+,u}$ is a saddle with two-dimensional stable manifold, for system (17).

We note

$$\xi^*_{+,s} = (1 + \tfrac{a}{b_1})\eta^*_{+,s} - \tfrac{a}{b_1} > (1 + \tfrac{a}{b})\eta^*_{+,s} - \tfrac{a}{b} = \gamma(\eta^*_{+,s}),$$

implying that $\mathbf{Q}^*_{+,s} \in S_-$. Such an equilibrium point is called a virtual equilibrium point [6], in the sense that $\mathbf{Q}^*_{+,s}$ cannot be "seen" by the vector field $\mathbf{V}_+$. A ϕ_+-trajectory in S_+ will intersect Σ (and switch to the flow ϕ_-) before having the chance to approach $\mathbf{Q}^*_{+,s}$.

Definition 5.1 Let $\mathbf{x}^* \in \mathcal{B}$.
(i) $\mathbf{x}^*$ is a *regular equilibrium point* of (19) if either $\mathbf{V}_+(\mathbf{x}^*) = \mathbf{0}$ and $\mathbf{x}^* \in S_+$, or if $\mathbf{V}_-(\mathbf{x}^*) = \mathbf{0}$ and $\mathbf{x}^* \in S_-$.
(ii) $\mathbf{x}^*$ is a *virtual equilibrium point* of (19) if either $\mathbf{V}_+(\mathbf{x}^*) = \mathbf{0}$ and $\mathbf{x}^* \in S_-$, or if $\mathbf{V}_-(\mathbf{x}^*) = \mathbf{0}$ and $\mathbf{x}^* \in S_+$.
(iii) $\mathbf{x}^*$ is a *boundary equilibrium point* of (19) if $\mathbf{V}_+(\mathbf{x}^*) = \mathbf{V}_-(\mathbf{x}^*) = \mathbf{0}$ and $\mathbf{x}^* \in \Sigma$.

The equilibrium point analysis for vector field $\mathbf{V}_-$ is similar. Note the Jacobian matrix $J_-(w, \eta, \xi)$ for (16) is identical to (20), except that b_1 is replaced with b_0 (observe $G'_+(\eta) = G'_-(\eta)$). As in [18], the decoupled (w, η)-block

$$M = \begin{bmatrix} -\tau & \tau F'(\eta) \\ \rho & -\rho G'_-(\eta) \end{bmatrix}$$

satisfies $\mathrm{Tr}(M) = -(\tau + \rho G'_-(\eta)) < 0$ for $\eta > 0$, while $\det(M) = -\tau\rho(F'(\eta) - G'_-(\eta))$. One can rigorously show the function $h_-(\eta) = F(\eta) - G_-(\eta)$ has two zeros $\eta^*_{-,u} < \eta^*_{-,s}$ in [0,1], with $h'_-(\eta^*_{-,u}) > 0$ and $h'_-(\eta^*_{-,s}) < 0$ (also see Figure 3). Thus subsystem (16a)-(16b) has a saddle point $(w^*_{-,u}, \eta^*_{-,u})$ and a sink $(w^*_{-,s}, \eta^*_{-,s})$ (see Figure 1(b)), from which it follows system (16) admits a saddle point $\mathbf{Q}^*_{-,u} = (w^*_{-,u}, \eta^*_{-,u}, \xi^*_{-,u})$ with two-dimensional stable manifold, and a sink $\mathbf{Q}^*_{-,s} = (w^*_{-,s}, \eta^*_{-,s}, \xi^*_{-,s})$. Once again the sink $\mathbf{Q}^*_{-,s}$ is virtual as

$$\xi^*_{-,s} = (1 + \tfrac{a}{b_0})\eta^*_{-,s} - \tfrac{a}{b_0} < (1 + \tfrac{a}{b})\eta^*_{-,s} - \tfrac{a}{b} = \gamma(\eta^*_{-,s}),$$

implying $\mathbf{Q}^*_{-,s} \in S_+$.

A key observation can be gleaned from Figure 1. First note subsystems (16a)-(16b) and (17a)-(17b) differ only in that $G_-(\eta) = G_+(\eta) + (T_c^- - T_c^+)$. As indicated in Figure 3, this simply moves $\eta^*_{-,u}$ and $\eta^*_{-,s}$ closer together, relative to $\eta^*_{+,u}$ and $\eta^*_{+,s}$. Also note $(w^*_{-,s}, \eta^*_{-,s})$ is in the stable set of $(w^*_{+,s}, \eta^*_{+,s})$ under the two-dimensional flow correspond-

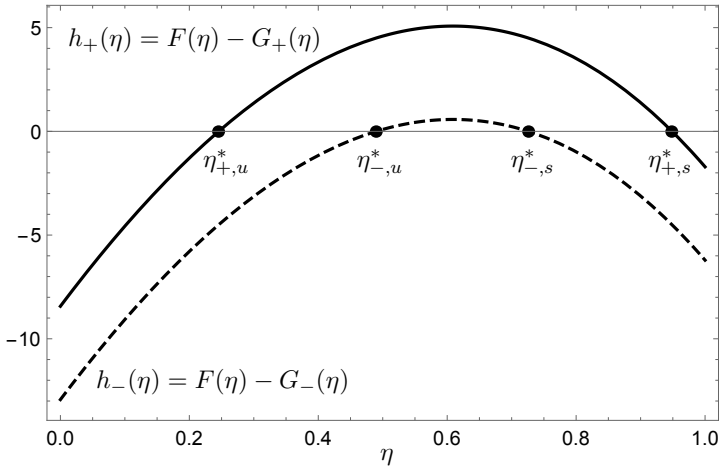

Figure 3: The η-coordinates at equilibrium. *Solid:* Subsystem (17a)-(17b), for which $T_c^+ = -10°\text{C}$. *Dashed:* Subsystem (16a)-(16b), for which $T_c^- = -5.5°\text{C}$.

ing to subsystem (17a)-(17b), while $(w^*_{+,s}, \eta^*_{+,s})$ is in the stable set of $(w^*_{-,s}, \eta^*_{-,s})$ under the two-dimensional flow corresponding to subsystem (16a)-(16b). Given the linear nature of equations (16c)-(17c) (along with the aforementioned decoupling), it follows that $\mathbf{Q}^*_{-,s}$ is in the stable set of $\mathbf{Q}^*_{+,s}$ under the flow ϕ_+ (system (17)), and $\mathbf{Q}^*_{+,s}$ is in the stable set of $\mathbf{Q}^*_{-,s}$ under the flow ϕ_- (system (16)).

More generally, the stable set of $(w^*_{-,s}, \eta^*_{-,s})$ under subsystem (16a)-(16b) is a subset of the stable set of $(w^*_{+,s}, \eta^*_{+,s})$ under subsystem (17a)-(17b). Thus the stable set of $\mathbf{Q}^*_{-,s}$ under the flow ϕ_- (system (16)) is a subset of the stable set of $\mathbf{Q}^*_{+,s}$ under the flow ϕ_+ (system (17)).

We now turn to the behavior of trajectories intersecting the discontinuity boundary Σ.

5.2 Behavior on the discontinuity boundary Σ

The discontinuity boundary Σ given by (18) is a plane with normal vector

$$\mathbf{N} = \begin{bmatrix} w & \eta & \xi \end{bmatrix}^T = \begin{bmatrix} 0 & 1 + \frac{a}{b} & -1 \end{bmatrix}^T.$$

For $\mathbf{x} \in \Sigma$, a computation yields $\mathbf{V}_+(\mathbf{x}) \perp \mathbf{N}$ if and only if

$$w = G_+(\eta) + \frac{\epsilon a(1-\eta)(b_1 - b)}{\rho(a+b)} \equiv g_+(\eta). \tag{21}$$

Thus $\mathbf{V}_+$ is tangent to Σ only on the parabola $\Lambda_+ = \{(w,\eta,\xi) \in \Sigma : w = g_+(\eta)\}$ (the red curve in Figure 4). Furthermore, given $\mathbf{x} = (w,\eta,\xi) \in \Sigma$, $\mathbf{V}_+(\mathbf{x})\cdot\mathbf{N} < 0$ for $w < g_+(\eta)$, and $\mathbf{V}_+(\mathbf{x})\cdot\mathbf{N} > 0$ for $w > g_+(\eta)$. Referring to the orientation provided in Figure 4, ϕ_+ trajectories pass through Σ below Λ_+ from front to back, while ϕ_+ trajectories pass through Σ above Λ_+ from back to front.

Similar computations reveal that $\mathbf{V}_-$ is tangent to Σ if and only if

$$w = G_-(\eta) + \frac{\epsilon a(1-\eta)(b_0 - b)}{\rho(a+b)} \equiv g_-(\eta), \tag{22}$$

that is, only on the parabola $\Lambda_- = \{(w,\eta,\xi) \in \Sigma : w = g_-(\eta)\}$ (the blue curve in Figure 4). Given $\mathbf{x} = (w,\eta,\xi) \in \Sigma$, $\mathbf{V}_-(\mathbf{x})\cdot\mathbf{N} > 0$ for $w > g_-(\eta)$, and $\mathbf{V}_+(\mathbf{x})\cdot\mathbf{N} < 0$ for $w < g_+(\eta)$. Thus ϕ_- trajectories pass through Σ below Λ_- from front to back, while ϕ_- trajectories pass through Σ above Λ_- from back to front.

Let

$$\Sigma^{\mathrm{SL}} = \{(w,\eta,\xi) \in \Sigma : g_+(\eta) < w < g_-(\eta)\}.$$

For $\mathbf{x} \in \Sigma^{\mathrm{SL}}$, $\mathbf{V}_+(\mathbf{x})\cdot\mathbf{N} > 0$ (so $\mathbf{V}_+(\mathbf{x})$ points into S_+), while $\mathbf{V}_-(\mathbf{x})\cdot\mathbf{N} < 0$ (so $\mathbf{V}_-(\mathbf{x})$ points into S_-). The subset Σ^{SL} of the discontinuity boundary Σ is therefore a *repelling sliding region* [15]; Filippov's approach does not provide for unique solutions $\mathbf{x}(t)$ in forward time if $\mathbf{x}(0) \in \Sigma^{\mathrm{SL}}$ [7].

Let

$$\Sigma_+ = \{(w,\eta,\xi) \in \Sigma : w < g_+(\eta)\} \quad \text{and} \quad \Sigma_- = \{(w,\eta,\xi) \in \Sigma : w > g_-(\eta)\}.$$

Unique solutions to (19) do exist for trajectories passing through Σ_+ or Σ_-, as $\mathbf{V}_-(\mathbf{x})\cdot\mathbf{N}$ and $\mathbf{V}_+(\mathbf{x})\cdot\mathbf{N}$ have the same sign on each of Σ_+ and Σ_-. A ϕ_+-trajectory in S_+ intersecting Σ_+ at $\mathbf{x}$ will cross Σ transversally, becoming a ϕ_--trajectory at $\mathbf{x}$. Similarly, a ϕ_--trajectory in S_- intersecting Σ_- at $\mathbf{y}$ will cross Σ transversally, becoming a ϕ_+-trajectory at $\mathbf{y}$. In this scenario a unique (though nonsmooth) solution of (19) exists, in the sense of Filippov.

5.3 Section maps for the Filippov flow

One can show the curves of tangency $\Lambda_\pm$ of $\mathbf{V}_\pm$ with Σ intersect precisely when

$$\eta = \eta(\epsilon) = 1 - \frac{(T_c^- - T_c^+)\rho(a+b)}{\epsilon a(b_1 - b_0)}. \tag{23}$$

Thus if

$$\epsilon < \frac{(T_c^- - T_c^+)\rho(a+b)}{a(b_1 - b_0)}, \tag{24}$$

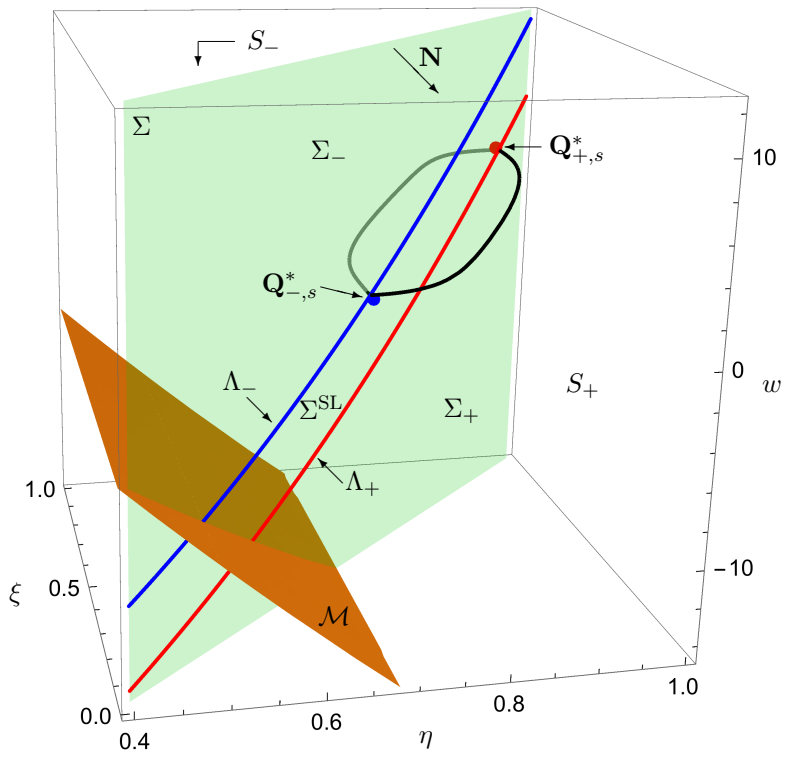

Figure 4: The discontinuity boundary Σ and domains $S_\pm$ for vector fields $\mathbf{V}_\pm$. $\mathbf{Q}^*_{-,s} \in S_+$ and $\mathbf{Q}^*_{+,s} \in S_-$ are virtual equilibria. Also pictured is the periodic orbit whose existence follows from Theorem 5.6.

$\eta(\epsilon)$ in (23) is strictly negative. We assume ϵ satisfies this bound in all that follows, ensuring Λ_+ and Λ_- do not intersect in $\mathcal{B}$ (as in Figure 4).

Plotted in Figure 4 is the two-dimensional stable manifold $\mathcal{M}$ of the saddle point $\mathbf{Q}^*_{-,u}$ under the flow ϕ_-. Due to the (w,η)-decoupling mentioned previously, the projection of $\mathcal{M}$ onto the (w,η)-plane is simply the (one-dimensional) stable manifold of $(w^*_{-,u}, \eta^*_{-,u})$ under the flow given by subsystem (16a)-(16b) and plotted in Figure 1(b). In particular, we note the plot of the surface $\mathcal{M}$ is independent of $\epsilon > 0$.

$\mathcal{M}$ partitions Σ into two subsets, a "top" (larger w) and a "bottom" (smaller w). Denote this top subset by $\mathcal{T}$. For any point $\mathbf{x} = (w,\eta,\xi) \in \mathcal{T}, \phi_-(\mathbf{x},t) = (w(t),\eta(t),\xi(t)) \to \mathbf{Q}^*_{-,s}$. This follows from the fact $(w(t),\eta(t)) \to (w^*_{-,s}, \eta^*_{-,s})$ as $t \to \infty$, and hence $\xi(t) \to \xi^*_{-,s}$ by equation (16c). Thus $\mathcal{T} \subset W^s_-(\mathbf{Q}^*_{-,s})$, the stable set of the sink $\mathbf{Q}^*_{-,s}$ under the flow ϕ_-. By the observations made in §5.1, it follows $\mathcal{T} \subset W^s_+(\mathbf{Q}^*_{+,s})$, the stable set of the sink $\mathbf{Q}^*_{+,s}$ under the flow ϕ_+. Again, all of this holds for any $\epsilon > 0$.

We have that for any $\epsilon > 0$, $\Sigma_+ \cap \mathcal{T} \subset W^s_-(\mathbf{Q}^*_{-,s})$ and $\mathbf{V}_-(\mathbf{x}) \cdot \mathbf{N} < 0$ for all $\mathbf{x} \in \Sigma_+ \cap \mathcal{T}$. Hence for any $\epsilon > 0$, the ϕ_--trajectory starting at $\mathbf{x} \in \Sigma_+ \cap \mathcal{T}$ enters S_- before necessarily intersecting $\Sigma_- \cap \mathcal{T}$ as it seeks to approach the (virtual) sink $\mathbf{Q}^*_{-,s}$. For any $\epsilon > 0$ and for each $\mathbf{x} \in \Sigma_+ \cap \mathcal{T}$, there is then a $t = t(\mathbf{x}) > 0$ such that $\phi_-(\mathbf{x}, t) \in \Sigma_- \cap \mathcal{T}$. We write $t(\mathbf{x}) = t(\mathbf{x}, \epsilon)$ to emphasize the dependence of this t-value on ϵ as well as on $\mathbf{x}$. We note, for future reference, that $t(\mathbf{x}, \epsilon) \to \infty$ as $\epsilon \to 0^+$.

This provides, for any $\epsilon > 0$, a continuous map

$$r^-_\epsilon : \Sigma_+ \cap \mathcal{T} \to \Sigma_- \cap \mathcal{T},\ r^-_\epsilon(\mathbf{x}) = \phi_-(\mathbf{x}, t(\mathbf{x}, \epsilon)).$$

Similarly, for any $\epsilon > 0$, $\Sigma_- \cap \mathcal{T} \subset W^s_+(\mathbf{Q}^*_{+,s})$ and $\mathbf{V}_+(\mathbf{y}) \cdot \mathbf{N} > 0$ for all $\mathbf{y} \in \Sigma_- \cap \mathcal{T}$. Hence for any $\epsilon > 0$, the ϕ_+-trajectory starting at $\mathbf{y} \in \Sigma_- \cap \mathcal{T}$ enters S_+ before necessarily intersecting $\Sigma_+ \cap \mathcal{T}$ as it tries to approach the (virtual) sink $\mathbf{Q}^*_{+,s}$. For any $\epsilon > 0$ and for each $\mathbf{y} \in \Sigma_- \cap \mathcal{T}$, there exists a $t = t(\mathbf{y}, \epsilon) > 0$ such that $\phi_+(\mathbf{y}, t) \in \Sigma_+ \cap \mathcal{T}$ (again, $t(\mathbf{y}, \epsilon) \to \infty$ as $\epsilon \to 0^+$). This defines a continuous map

$$r^+_\epsilon : \Sigma_- \cap \mathcal{T} \to \Sigma_+ \cap \mathcal{T},\ r^+_\epsilon(\mathbf{y}) = \phi_+(\mathbf{y}, t(\mathbf{y}, \epsilon)),$$

which exists for any $\epsilon > 0$.

We then have two continuous section maps

$$r^+_\epsilon \circ r^-_\epsilon : \Sigma_+ \cap \mathcal{T} \to \Sigma_+ \cap \mathcal{T} \ \text{ and } \ r^-_\epsilon \circ r^+_\epsilon : \Sigma_- \cap \mathcal{T} \to \Sigma_- \cap \mathcal{T}, \tag{25}$$

each defined for any $\epsilon > 0$. Given certain hypotheses, these maps are each contraction maps, as we show in the following section.

5.4 Existence of an attracting periodic orbit

We begin with the following propositions.

Proposition 5.4 (i) Given $c_1 \in (0, 1)$ and a compact set $D_+ \subset \Sigma_+ \cap \mathcal{T}$, there exists $\epsilon_1 > 0$ such that for all $\epsilon \le \epsilon_1$ and for all $\mathbf{x}_1, \mathbf{x}_2 \in D_+$, $\|r^-_\epsilon(\mathbf{x}_2) - r^-_\epsilon(\mathbf{x}_1)\| \le c_1 \|\mathbf{x}_2 - \mathbf{x}_1\|$.

(ii) Given $c_2 \in (0, 1)$ and a compact set $D_- \subset \Sigma_- \cap \mathcal{T}$, there exists $\epsilon_2 > 0$ such that for all $\epsilon \le \epsilon_2$ and for all $\mathbf{y}_1, \mathbf{y}_2 \in D_-$, $\|r^+_\epsilon(\mathbf{y}_2) - r^+_\epsilon(\mathbf{y}_1)\| \le c_2 \|\mathbf{y}_2 - \mathbf{y}_1\|$.

Proof. We prove (i). Let $c_1 \in (0, 1)$ and let $D_+ \subset \Sigma_+ \cap \mathcal{T}$, D_+ compact. Let ψ_- denote the flow corresponding to subsystem (16a)-(16b) (with phase plane depicted in Figure 1(b)). For any $\mathbf{x} = (w_0, \eta_0, \xi_0) \in D_+ \subset \mathcal{T}$, $\psi_-((w_0, \eta_0), t) \to (w^*_{-,s}, \eta^*_{-,s})$ as $t \to \infty$. As $E = \{(w, \eta) : (w, \eta, \xi) \in D_+\}$ is compact, there exists T_1 such that for all $t \ge T_1$ and for

all $\mathbf{u}, \mathbf{v} \in E$,

$$\|\psi_-(\mathbf{u}, t) - \psi_-(\mathbf{v}, t)\| \leq c_1 \|\mathbf{u} - \mathbf{v}\|. \tag{26}$$

Given $\mathbf{x} \in D_+$, pick $\epsilon(\mathbf{x}) > 0$ such that $t(\mathbf{x}, \epsilon(\mathbf{x})) > T_1$ (recalling $\phi_-(\mathbf{x}, t(\mathbf{x}, \epsilon(\mathbf{x}))) = r^-_{\epsilon(\mathbf{x})}(\mathbf{x}) \in \Sigma_- \cap \mathcal{T}$).

By the continuity of ϕ_- with respect to initial conditions and time, there exists $\delta(\mathbf{x}) > 0$ so that for all $\mathbf{y} \in B_{\delta(\mathbf{x})}(\mathbf{x}),\ t(\mathbf{y}, \epsilon(\mathbf{x})) > T_1$, where $r^-_{\epsilon(\mathbf{x})}(\mathbf{y}) \in \Sigma_- \cap \mathcal{T}$. Note for all $\epsilon \leq \epsilon(\mathbf{x}), t(\mathbf{y}, \epsilon) > T_1$.

Letting $\mathbf{x}$ vary, we get an open covering

$$D_+ \subset \bigcup_{\mathbf{x} \in D_+} B_{\delta(\mathbf{x})}(\mathbf{x})$$

of the compact set D_+. Let $\{B_{\delta(\mathbf{x}_i)}(\mathbf{x}_i) : i = 1, ..., N\}$ be a finite subcover, and set $\epsilon_1 = \min\{\epsilon(\mathbf{x}_i) : i = 1, ..., N\}$. Then for any $\epsilon \leq \epsilon_1$ and for all $\mathbf{x} \in D_+,\ t(\mathbf{x}, \epsilon) > T_1$, where $r^-_\epsilon(\mathbf{x}) \in \Sigma_- \cap \mathcal{T}$.

Now let $\epsilon \leq \epsilon_1$, and let $\mathbf{x}_1 = (w_1, \eta_1, \gamma(\eta_1)), \mathbf{x}_2 = (w_2, \eta_2, \gamma(\eta_2)) \in D_+$. Set $\mathbf{u} = (w_1, \eta_1)$ and $\mathbf{v} = (w_2, \eta_2)$. Let $\mathbf{y}_1 = r^-_\epsilon(\mathbf{x_1}) = (w_1', \eta_1', \gamma(\eta_1'))$ and $\mathbf{y}_2 = r^-_\epsilon(\mathbf{x_2}) = (w_2', \eta_2', \gamma(\eta_2'))$. Set $\mathbf{u}' = (w_1', \eta_1')$ and $\mathbf{v}' = (w_2', \eta_2')$. By (26) and our choice of ϵ, $\|\mathbf{v}' - \mathbf{u}'\|^2 \leq c_1^2 \|\mathbf{v} - \mathbf{u}\|^2$. We have

$$\begin{aligned}
\|\mathbf{y}_2 - \mathbf{y}_1\|^2 &= \|\mathbf{v}' - \mathbf{u}'\|^2 + (\gamma(\eta_2') - \gamma(\eta_1'))^2 \\
&= \|\mathbf{v}' - \mathbf{u}'\|^2 + (1 + \tfrac{a}{b})^2 (\eta_2' - \eta_1')^2 \\
&\leq c_1^2 \|\mathbf{v} - \mathbf{u}\|^2 + (1 + \tfrac{a}{b})^2 c_1^2 (\eta_2 - \eta_1)^2 \\
&= c_1^2 \|\mathbf{v} - \mathbf{u}\|^2 + c_1^2 (\gamma(\eta_2) - \gamma(\eta_1))^2 \\
&= c_1^2 \|\mathbf{x}_2 - \mathbf{x}_1\|^2.
\end{aligned}$$

Hence statement (i) holds. The proof of statement (ii) is similar. □

To use Proposition 5.4 to show that, say, $r^+_\epsilon \circ r^-_\epsilon$ is a contraction map, we need a compact set $D_+ \subset \Sigma_+ \cap \mathcal{T}$ such that $r^+_\epsilon \circ r^-_\epsilon(D_+) \subset D_+$. To that end, let $\mathbf{Z}^*_+ = (w^*_{+,s}, \eta^*_{+,s}, \gamma(\eta^*_{+,s}))$, and note $\mathbf{Z}^*_+ \in \mathcal{T} \cap \Sigma = \mathcal{T}$. Moreover, that $\mathbf{Z}^*_+ \in \Sigma_+$ follows from the fact $w^*_{+,s} = G_+(\eta^*_{+,s}) < g_+(\eta^*_{+,s})$, which in turn is a consequence of (21).

Similarly, let $\mathbf{Z}^*_- = (w^*_{-,s}, \eta^*_{-,s}, \gamma(\eta^*_{-,s})) \in \mathcal{T}$. As $w^*_{-,s} = G_-(\eta^*_{-,s}) > g_-(\eta^*_{-,s})$ by equation (22), we have $\mathbf{Z}^*_- \in \Sigma_-$.

Proposition 5.5 (i) Let D_+ be any compact subset of $\Sigma_+ \cap \mathcal{T}$ with $\mathbf{Z}^*_+ \in \mathrm{Int}(D_+)$. Let D_- be any compact subset of $\Sigma_- \cap \mathcal{T}$. There exists $\epsilon_3 > 0$ such that for all $\epsilon \leq \epsilon_3,\ r^+_\epsilon(D_-) \subset D_+$.

(ii) Let D_- be any compact subset of $\Sigma_- \cap \mathcal{T}$ with $\mathbf{Z}_-^* \in \text{Int}(D_-)$. Let D_+ be any compact subset of $\Sigma_+ \cap \mathcal{T}$. There exists $\epsilon_4 > 0$ such that for all $\epsilon \leq \epsilon_4$, $r_\epsilon^-(D_+) \subset D_-$.

Proof. We prove (i). Let $\mathbf{x} = (w_0, \eta_0, \gamma(\eta_0)) \in D_-$. Pick $\delta > 0$ such that $U_{2\delta} = B_{2\delta}(\mathbf{Z}_+^*) \cap \Sigma \subset D_+$. Let ψ_+ denote the flow corresponding to subsystem (17a)-(17b). Note $\psi_+((w_0, \eta_0), t) = (w(t), \eta(t)) \to (w_{+,s}^*, \eta_{+,s}^*)$ as $t \to \infty$. Additionally noting $\gamma(\eta)$ is continuous, there exists $T = T(\mathbf{x}) > 0$ such that for all $t \geq T$,

$$\|(w(t), \eta(t), \gamma(\eta(t))) - \mathbf{Z}_+^*\| < \delta.$$

Pick $\epsilon(\mathbf{x}) > 0$ such that $t(\mathbf{x}, \epsilon(\mathbf{x})) > T$ (recalling $\phi_+(\mathbf{x}, t(\mathbf{x}, \epsilon(\mathbf{x}))) = r_{\epsilon(\mathbf{x})}^+(\mathbf{x})$). Then for all $\epsilon \leq \epsilon(\mathbf{x})$, $r_\epsilon^+(\mathbf{x}) \in B_\delta(\mathbf{Z}_+^*) \cap \Sigma$.

Let $c_2 \in (0,1)$, $c_2 < \delta/\text{diam}(D_-)$. Pick $\epsilon_2 > 0$ as in Proposition 5.3(ii). Let $\epsilon_3 = \min\{\epsilon(\mathbf{x}), \epsilon_2\}$. For $\epsilon \leq \epsilon_3$ and $\mathbf{y} \in D_-$,

$$\|r_\epsilon^+(\mathbf{y}) - r_\epsilon^+(\mathbf{x})\| \leq c_2 \|\mathbf{y} - \mathbf{x}\| \leq c_2 \text{ diam}(D_-) < \delta,$$

implying

$$\|r_\epsilon^+(\mathbf{y}) - \mathbf{Z}_+^*\| \leq \|r_\epsilon^+(\mathbf{y}) - r_\epsilon^+(\mathbf{x})\| + \|r_\epsilon^+(\mathbf{x}) - \mathbf{Z}_+^*\| < 2\delta.$$

Hence, $r_\epsilon^+(D_-) \subset U_{2\delta} \subset D_+$. The proof of (ii) is similar. □

Theorem 5.6 With parameters as in Table 1, there exists $\hat{\epsilon} > 0$ so that for all $\epsilon \leq \hat{\epsilon}$, system (19) admits an attracting periodic orbit.

Remark. This result holds more generally for any $0 < b_0 < b < b_1$, and for any $\tau > 0$ and $\rho > 0$.

Proof. Let $D_+ \subset \Sigma_+ \cap \mathcal{T}$, with D_+ compact and $\mathbf{Z}_+^* \in \text{Int}(D_+)$. Let $D_- \subset \Sigma_- \cap \mathcal{T}$, with D_- compact and $\mathbf{Z}_-^* \in \text{Int}(D_-)$. Given $c_1 \in (0,1)$, pick $\epsilon_1 > 0$ such that for all $\epsilon \leq \epsilon_1$ and for all $\mathbf{x}_1, \mathbf{x}_2 \in D_+$,

$$\|r_\epsilon^-(\mathbf{x}_2) - r_\epsilon^-(\mathbf{x}_1)\| \leq c_1 \|\mathbf{x}_2 - \mathbf{x}_1\|.$$

Given $c_2 \in (0,1)$, pick $\epsilon_2 > 0$ such that for all $\epsilon \leq \epsilon_2$ and for all $\mathbf{y}_1, \mathbf{y}_2 \in D_-$,

$$\|r_\epsilon^+(\mathbf{y}_2) - r_\epsilon^+(\mathbf{y}_1)\| \leq c_2 \|\mathbf{y}_2 - \mathbf{y}_1\|.$$

Pick $\epsilon_3 > 0$ such that for all $\epsilon \leq \epsilon_3$, $r_\epsilon^+(D_-) \subset D_+$, and choose $\epsilon_4 > 0$ such that for all $\epsilon \leq \epsilon_4$, $r_\epsilon^-(D_+) \subset D_-$.

For $\epsilon \leq \hat{\epsilon} = \min\{\epsilon_1, \epsilon_2, \epsilon_3, \epsilon_4\}$,

$$r_\epsilon = r_\epsilon^+ \circ r_\epsilon^- : D_+ \to D_+$$

is a contraction map with contraction factor $c_1 c_2 \in (0, 1)$. Hence r_ϵ has a unique fixed point $\mathbf{x}^*$ to which all r_ϵ-orbits in D_+ converge. Flowing via ϕ_- from $\mathbf{x}^*$ to $r_\epsilon^-(\mathbf{x}) = \mathbf{y}^*$, and via ϕ_+ from $\mathbf{y}^*$ to $r_\epsilon^+(\mathbf{y}^*) = \mathbf{x}^*$, provides the desired periodic orbit. Every Filippov trajectory of system (19) passing through D_+ converges to this limit cycle. □

In Figure 5 we present the periodic behavior of the model for three ϵ-values. When ϵ is two orders of magnitude smaller than ρ, w and η move so quickly relative to ξ that they essentially switch from a point near $(w^*_{+,s}, \eta^*_{+,s})$ to a point near $(w^*_{-,s}, \eta^*_{-,s})$, and vice versa (Figure 5, top row). This is the essence of the idea behind the proof of Theorem 5.6.

The middle panel in Figure 5 illustrates the periodic behavior when ϵ is one order of magnitude smaller than ρ. Interestingly, the limit cycle persists when ϵ and ρ have the same order of magnitude (Figure 5, bottom row).

6 Conclusion

Building on previous work [5], [33], [18], we separated the classic Budyko ice line into two dynamic variables, the snow line and the glacial boundary, producing a system of three ordinary differential equations. Introducing two distinct climate states, one corresponding to glacial advance and the other to glacial retreat, we formulated the equations as a Filippov system with a two-dimensional plane forming the discontinuity boundary.

For the parameter values of interest here, the system has two virtual attracting equilibria, one for each of the two climate states. For example, starting with a climate where the glaciers are retreating, the system moves toward its virtual equilibrium, crossing the discontinuity boundary before reaching it. Upon crossing the boundary, the system switches climate regimes and starts heading toward the virtual equilibrium for advancing glaciers. Again, the virtual equilibrium cannot be reached and the orbit crosses the discontinuity boundary, switching back to retreating glaciers. This behavior is analogous to that found in the Welander model [32], and it produces a periodic orbit.

The proof of the existence of this periodic orbit uses ad-hoc singular perturbation techniques, with ϵ as the singular parameter. Recall that ϵ controls the speed at which the orbit approaches the discontinuity boundary Σ. By taking ϵ small enough, we were able to control the contraction parameter, giving a unique attracting fixed point for the section map, corresponding to an attracting periodic orbit for the system of differential

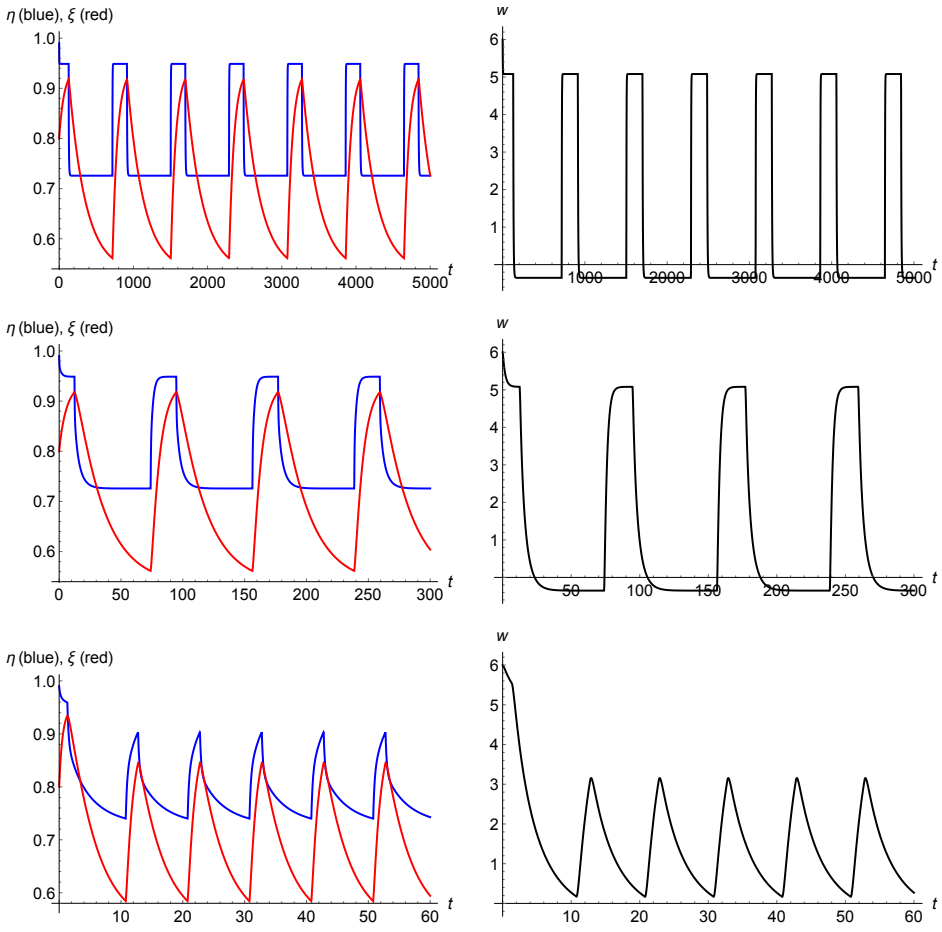

Figure 5: Periodic behavior for system (19). *Top:* $\epsilon = 0.003$. *Middle:* $\epsilon = 0.03$. *Bottom:* $\epsilon = 0.3$. In each plot $\tau = 1$ and $\rho = 0.1$, with other parameters given in Table 1.

equations. This periodic orbit represents an intrinsic cycling of the climate systems, producing the glacial cycles.

We view our analysis as suggesting the need for a general theory of singular perturbations for Filippov systems.

We also view our model as providing a first step toward a conceptual model of the Earth's glacial cycles. We chose parameters so that the system has two virtual equilibria, giving us an intrinsic oscillation. A next step would be to incorporate the Milankovitch cycles into the model. This would be easily accomplished, since the parameter Q in equation (1) depends on the eccentricity while the parameter s_2 in equation (4) depends

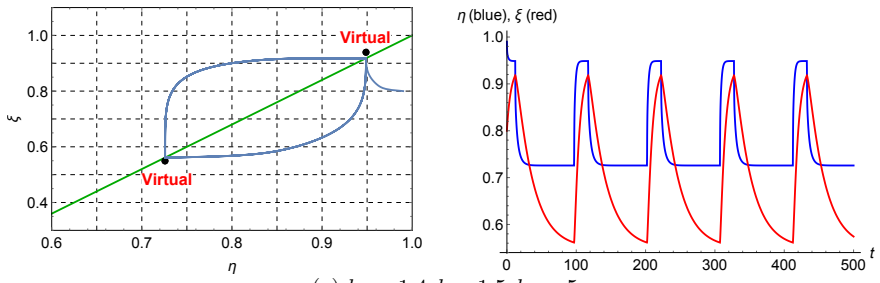

(a) $b_0 = 1.4, b = 1.5, b_1 = 5$.

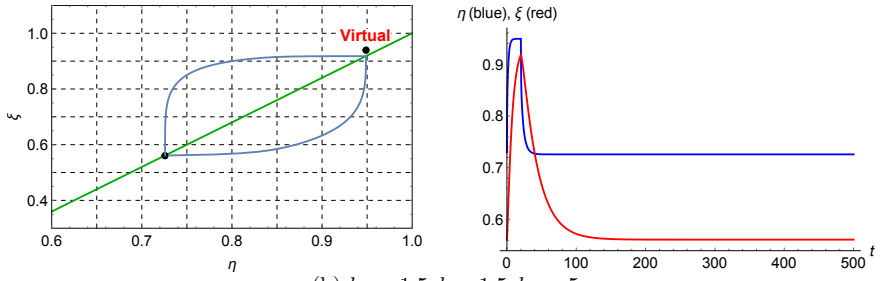

(b) $b_0 = 1.5, b = 1.5, b_1 = 5$.

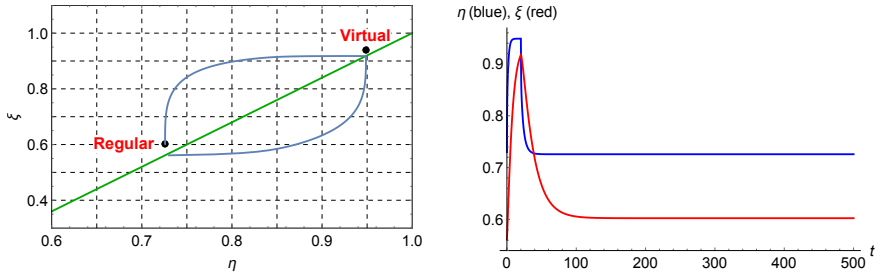

(c) $b_0 = 2, b = 1.5, b_1 = 5$.

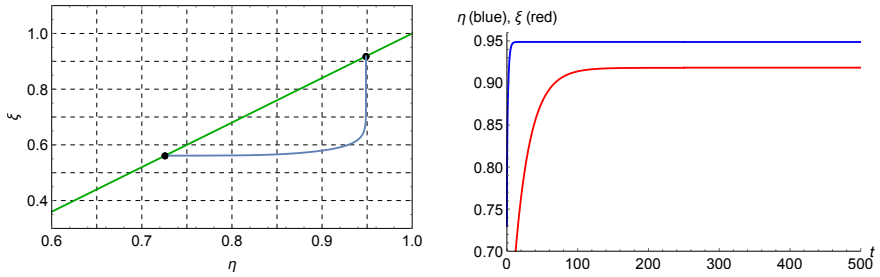

(d) $b_0 = 1.5, b = 1.5, b_1 = 1.5$.

Figure 6: Illustration of a boundary equilibrium bifurcation as b_0 increases through b. Plotted are projections of various orbits onto the (η, ξ)-plane, and the corresponding $\eta(t)$ and $\xi(t)$ graphs. (a) Limit cycle. (b) $\mathbf{Q}^*_{-,s} \in \Sigma$. (c) $\mathbf{Q}^*_{-,s} \in S_-$. (d) $\mathbf{Q}^*_{-,s}, \mathbf{Q}^*_{+,s} \in \Sigma$.

on the obliquity [17]. As these parameters vary with the Milankovitch cycles, the system might be nudged across the discontinuity boundary, creating a resonance with either eccentricity or obliquity.

Other directions suggested by this model are more mathematical in nature. For example, both of the virtual equilibria are close to the discontinuity boundary for the parameters we chose. By adjusting the parameters, one could produce a boundary equilibrium bifurcation for one or both of the equilibria (see Figure 6). As one of the virtual equilibria crossed the discontinuity boundary, the periodic orbit would presumably disappear and be replaced by an attracting rest point. Moving the parameters in the other direction would find the system dramatically changing from an attracting equilibrium to a large oscillation, reminiscent of the phenomenon used by Maasch and Salzman to explain the mid-Pleistocene transition [16].

The mid-Pleistocene transition is a period roughly 1 million years ago when the length of the glacial-interglacial cycles changed from approximately 40,000 years to 100,000 years. Substantial efforts have been made to solve this "100,000 year problem" (see, for example, [2], [12], [22], [24], [29]). One might allow the parameters to vary in our model to see whether this transition can be realized. Comparisons can be made between model output and the paleoclimate data.

Again returning to mathematical questions, it would be interesting to explore the parameter space with the goal of discovering the origin of the periodic orbit we exhibited. Perhaps the orbit originated with a classic Hopf bifurcation, or perhaps it originated with bifurcation from a "fused focus" as discussed by Filippov [7]. These explorations may or may not have implications for interpretation of the paleoclimate data, but they will almost certainly lead to interesting examples of bifurcations in Filippov systems.

Conceptual in nature, the simple model introduced here gives rise to a host of problems deserving of further study.

Acknowledgment. The authors recognize and appreciate the support of the Mathematics and Climate Research Network (www.mathclimate.org). The work was partially supported by NSF Grants DMS-0940366 and DMS-0940363.

References

[1] A. Abe-Ouchi, F.Saito, K. Kawamura, M.E. Raymo, J. Okuno, K. Takahashi and H. Blatter, Insolation-driven 100,000-year glacial cycles and hysteresis of ice-sheet volume, *Nature* **500** (2013), 190-194.

[2] P. Ashwin and P. Ditlevsen, The middle Pleistocene transition as a generic bifurcation on a slow manifold, *Climate Dynamics*, published online February 14, 2015.

[3] D. Bahr, M. Meier and S. Peckham, The physical basis of glacier volume-area scaling, *J. Geophys. Res.* **102** (1997), 20,355-20,362.

[4] C. Bøggild, R. Brandt, K. Brown and S. Warren, The ablation zone in northeast Greenland: ice types, albedos and impurities, *J. Glaciology* **56** (195) (2010), 101-113.

[5] M. I. Budyko, The effect of solar radiation variation on the climate of the Earth, *Tellus* **5** (1969), 611–619.

[6] M. di Bernardo, C. Budd, A. Champneys, P. Kowalczyk, A. Nordmark, G. Tost and P. Piiroinen, Bifurcations in nonsmooth dynamical systems, *SIAM Review* **50** (4) (2008), 629-701.

[7] A.F. Filippov, Differential equations with discontinuous right-hand side, *Amer. Math. Soc. Trans. Ser. 2*, **42** (1964), 199-123.

[8] M. Ghil and H. LeTreut, A climate model with cryodynamics and geodynamics, *J. Geophys. Res.* **86** (1981), 5262-5270.

[9] J. Guckenheimer, Review of the book *Piecewise-Smooth Dynamical Systems* by M. di Bemardo, C.J. Budd, A.R. Champneys, and P. Kowalczyk, *SIAM Review* **50** (3) (2008), 606-609.

[10] J. D. Hays, John Imbrie, and N. J. Shackleton, Variations in the Earth's orbit: pacemaker of the ice ages, *Science* **194** (4270) (1976), 1121-1132.

[11] I. Held and M. Suarez, Simple albedo feedback models of the icecaps, *Tellus* **26** (1974), 613-629.

[12] P. Huybers, Glacial variability over the last two million years: An extended depth-derived agemodel, continuous obliquity pacing, and the Pleistocene progression, *Quaternary Science Reviews* **26** (1-2) (2007), 37-55.

[13] P. Huybers, Combined obliquity and precession pacing of late Pleistocene deglaciations, *Nature* **480** (2011), 229-232.

[14] E. Källén, C. Crafoord and M. Ghil, Free oscillations in a climate model with ice-sheet dynamics, *J. Atmos. Sci.* **36** (1979), 2292-2303.

[15] R.I. Leine and H. Nijmeijer, *Dynamics and Bifurcations of Non-smooth Mechanical Systems*, Springer-Verlag, Berlin, Germany and New York, NY, USA, 2004.

[16] K. Maasch and B. Saltzman, A low-order dynamical model of global climatic variability over the full Pleistocene, *J. Geophys. Res.*, **95** (D2) (1990), 1955-1963.

[17] R. McGehee and C. Lehman, A paleoclimate model of ice-albedo feedback forced by variations in Earth's orbit, *SIAM J. Appl. Dyn. Syst.* **11** (2012), 684–707.

[18] R. McGehee and E. Widiasih, A quadratic approximation to Budyko's ice-albedo feedback model with ice line dynamics, *SIAM J. Appl. Dyn. Syst.* **13** (2014), 518-536.

[19] M. Milankovitch, Canon of Insolation and the Ice-age Problem (Kanon der Erdbestrahlung und seine Anwendung auf das Eiszeitenproblem, Belgrade, 1941), Israel Program for Scientific Translations, Jerusalem, 1969.

[20] G. North, Theory of energy-balance climate models, *J. Atmos. Sci.* **32** (1975), 2033–2043.

[21] J. Oerlemans, Glacial cycles and ice sheet modeling, *Climate Change* **4** (1982), 353-374.

[22] D. Paillard, The timing of Pleistocene glaciations from a simple multiple-state climate model, *Nature* **391** (4270) (1998), 378-381.

[23] D. Paillard and F. Parrenin, The Antarctic ice sheet and the triggering of deglaciations, *Earth and Planetary Science Letters* **227** (2004), 263-271.

[24] F. Parrenin and D. Paillard, Amplitude and phase of glacial cycles from a conceptual model, *Earth and Planetary Science Letters* **214** (2003), 243-250.

[25] W.R. Peltier and S. Marshall, Coupled energy-balance/ice-sheet model simulations of the glacial cycle: A possible connection between terminations and terrigenous dust, *J. Geophys. Res.* **100** (1995), 14,269-14,289.

[26] J. R. Petit, J. Jouzel, D. Raynaud, N. I. Barkov, J.-M. Barnola, I. Basile, M. Bender, J. Chappellaz, M. Davisk, G. Delaygue, M. Delmotte, V. M. Kotlyakov, M. Legrand, V. Y. Lipenkov, C. Lorius, L. Pépin, C. Ritz, E. Saltzmank and M. Stievenard, Climate and atmospheric history of the past 420,000 years from the Vostok ice core, Antarctica, *Nature* **399** (1999), 429–436.

[27] W. Ruddiman, Orbital changes and climate, *Quaternary Science Reviews* **25** (2006), 3092-3112.

[28] W. Sellers, A global climatic model based on the energy balance of the Earth-Atmosphere system, *J. Appl. Meteor.*, **8** (1969), 392–400.

[29] E. Tziperman and H. Gildor, On the mid-Pleistocene transition to 100-kyr glacial cycles and the asymmetry between glaciation and deglaciation times, *Paleoceanography* **18** (1) (2003).

[30] J.A. Walsh and C. Rackauckas, On the Budyko-Sellers energy balance climate model with ice line coupling, *Disc. Cont. Dyn. Syst. B* **20** (7) (2015).

[31] J. Weertman, Milankovitch solar radiation variations and ice age ice sheet sizes, *Nature* **261** (1976), 17-20.

[32] P. Welander, A simple heat-salt oscillator, *Dyn. Atmosph. Oceans* **6** (1982), 233-242.

[33] E. Widiasih, Dynamics of the Budyko energy balance model, *SIAM J. Appl. Dyn. Syst.* **12** (2013), 2068-2092.

[34] H. Wright and I. Stefanova, Plant trash in the basal sediments of glacial lakes, *Acta Palaeobotanica* **44** (2) (2004), 141-146.